



Detection of dust storms overnight in the South West of Iran using satellite images

Marziyeh Deiravipour¹, Hossein Mohammad Asgari^{1,*}, Saeid Farhadi¹

¹ Marine Environment, Department of Marine Natural Resources, Khorramshahr University of Marine Science and Technology, Khuzestan, Iran

Received: 13 January 2021, Revised: 08 August 2021, Accepted: 18 August 2021

© University of Tehran

Abstract

Dust concentration, as the level of particulate matter (PM10), has become an important indicator of air pollution, and has attracted a great deal of attention from environmental agencies and organizations, public health, and science worldwide. Over recent years, dust storms with intense drought have had numerous adverse effects on human health and socio-economic situation in arid and semi-arid countries. Despite the inevitability of their occurrence, natural and human activities could exacerbate this phenomenon. Imagery data analyses have improved our understanding of dust detection and monitoring. Previous research has extensively studied the dust storms in day time. Meanwhile, there are a few studies investigating dust detection over-night. For dust detection over-night, several algorithms were utilized herein, including brightness temperature difference (BTD) for 20, 23, 31, and 32 MODIS bands and artificial neural network (ANN). The obtained results revealed that BTD indices have good performance for dust detection in the southwest of Iran and their accuracy will be better with an increase in the concentration and density of dust and a reduction in cloud cover in the region. The BTD and ANN methods were evaluated using different indices. Our findings revealed that ANN method was more accurate than BTD indices. This finding is probably attributed to the complex properties of dust; artificial neural network is an appropriate method to model nonlinear and complex dust and surface properties.

Keywords: Dust, MODIS, Brightness temperature difference (BTD), Artificial neural network (ANN)

Introduction

Dust concentration, characterized by the level of particulate matter (PM10), has become an important indicator of air pollution, and has attracted a great deal of attention from environmental agencies and organizations, public health, and science worldwide (Li et al., 2020). Previous studies have shown that the risk of poisoning with PM10 concentrations on dusty days is more than that on clean days due to further inhalation of dust in the atmosphere (Naimabadi et al., 2016). Inhabitants in the vicinity of dust sources are the most prone to a high risk of the adverse effects caused by storms (Bahrami, et al., 2020). Although the occurrence of dust storms is inevitable, it could aggravate as a consequence of natural and human reasons. To identify dust storms, Synoptic and imagery analyses are essential (Boroughani, et al., 2020). Since dust can directly change sunlight in both visible and infrared spectral regions through the dispersion and absorption process, visible and infrared remote sensing techniques can be used to detect dust particles in the atmosphere (Shi et al., 2020). In order to better understand the effects of dust, their concentration and size should be regularly monitored on a global scale, which is difficult in practice since fine particles of dust have high

* Corresponding author e-mail: h.masgari@kmsu.ac.ir

spatial and temporal variations. Through the use of land measurement stations, we can obtain information about dust. Nonetheless, due to the complexity of the process of measuring the characteristics of these microparticles, the establishment and maintenance of these stations are costly (Nabavi, 2016). To detect dust, in situ methods are time-consuming, cost-inefficient, and labor intensive. However, remote sensing offers up-to-date, cost-effective, and large coverage of vast areas. Remote sensing techniques such as dust detection algorithms have been developed with regard to use in other atmospheric and terrestrial phenomena (Hou et al., 2020). The climatic conditions of various regions affect the intensity and duration of dust storms. Numerous researchers from different parts of the world have studied these storms at different times of the day, but there is scarce research on dust detection over-night (El-Ossta, 2013).

Many papers in Iran and around the world have investigated the trace of sand and detected dust from clouds and sediments using BTD parameter, TIDI index, and the difference between brightness temperature of 20, 23, 29, 30, 31, and 32 bands of MODIS in day time. This method has been reported to be suitable for detecting dust and determining the extent and severity of storms, and is capable of detecting dust storms in non-sandy fields. However, it is not suitable for sandy soils, like the Sahara. It has been also reported that there is a difference between the ground, storm dust, cloud, and snow if the dust concentration is low, but the diagnosis does not work well (Komeilian et al., 2014; Cao et al., 2015; Park et al., 2013). A number of studies have indicated that the detection of dust would be more accurate if the threshold was determined more carefully; for example, Huang et al. (2007) utilized the difference in the brightness of the 11th and 12th bands of MODIS sensor. Their results showed that the difference in brightness temperature with threshold (-2) could detect 80% of dust storms and 5% of the clouds in the region. The threshold (-1) could detect 98% of the dust and 15% of the clouds (Huang et al., 2007). Moreover, some studies have shown that the detection of dust on bright surfaces faces certain limitations; for instance, Zhao et al. (2010) employed 0.47, 0.64, 0.86, 1.38, 2.26, 3.9, 11, and 12 micrometers of MODIS sensors to detect dust throughout a day. They reported that this algorithm is efficiently able to detect heavy dust in aquatic and drought ecosystems; meanwhile, due to relatively weak signals of dust and ambiguity in detecting bright surfaces, it is not able to determine the thickness and dispersion of dust (Zhao et al., 2010). Yang et al. (2017) used satellite imagery and feature of various phenomena, such as cloud, vegetation, ice/snow, for analyzing the temperature and detecting dust, whose results were compared with true color combinations (Yang et al., 2017).

Several investigations have been conducted on automatic detection of dust using the artificial neural network (ANN) method. In this regard, the current work aimed to classify and increase ANN accuracy through the use of thermal band, including 20, 29, 31, and 32 bands of MODIS sensors, as well as sample images of various phenomena, such as dust, vegetation, and land. Previous studies show that neural network is an appropriate method for detecting dust and estimating the concentration of PM (Lee et al., 2020; Xiao et al., 2015; El-Ossta, 2013; Wu et al., 2012; Chacon-Murguía et al., 2011).

Herein, MODIS data were used in order to address the following questions: 1) Are the MODIS images capable of detecting dust over-night? 2) Which BTD indices have higher accuracy for dust detection? 3) What is the advantage of using artificial neural network method?

Materials and Methods

Study area

The main objective of this study was to investigate dust storms in the southwest of Iran, which mainly originated from the dry and desert regions of the neighboring countries, such as Iraq, Syria, and Saudi Arabia. The abundance of very fine and light particles, such as silt, clay, and sand, in the desert areas of the neighboring countries as well as the wind blowing from these areas to the western and southwest provinces of Iran lead to dust storms (Kamaland et al., 2019).

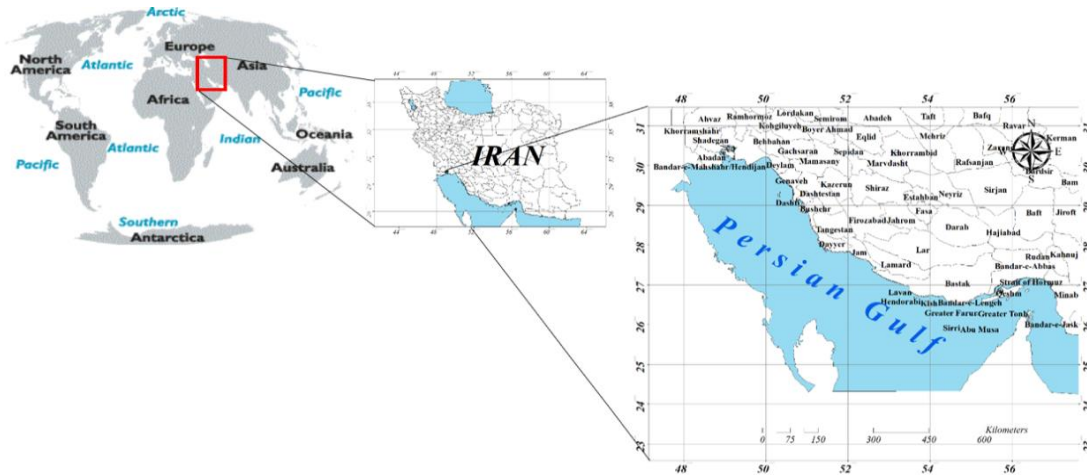


Figure 1. Study area

Methodology

In this study, Terra MOD02 and Aqua MYD02 datasets were used and processed with MATLAB and ENVI software. Among the 36 channels of MODIS, the visible and near infrared channels were used to measure the objects' reflection while the thermal infrared channels were utilized to measure the objects' brightness temperature (Mei et al., 2008). Figure 2 represents the methodology flowchart for brightness temperature difference (BTD) and artificial neural network (ANN) approaches.

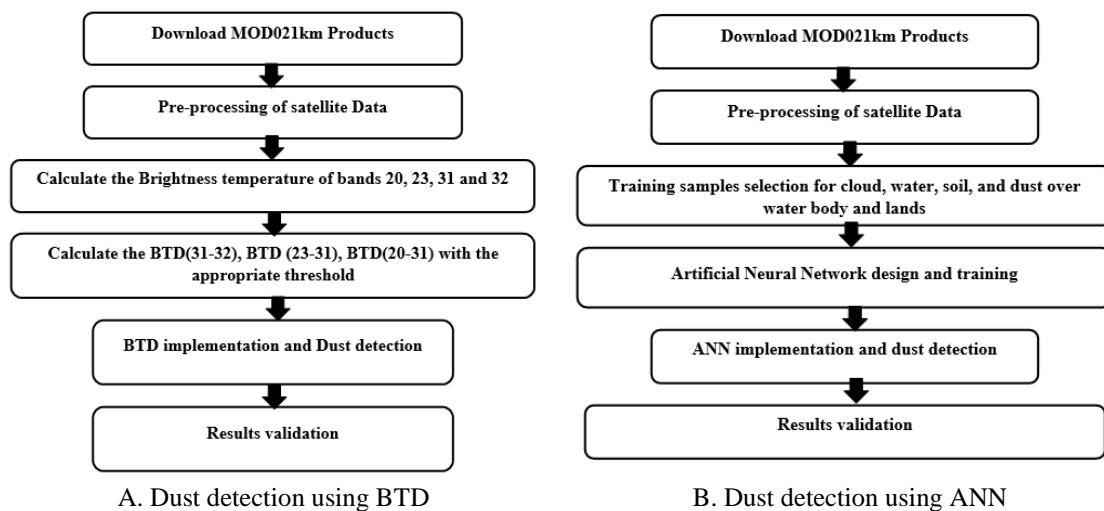


Figure 2. Methodology flowchart

Typically, infrared bands are employed to detect dust and calculate the brightness temperature of water, earth, and atmospheres with different thresholds. Brightness temperature difference between channels 31 and 32 has been used in many studies. Brightness temperature of dust storms in the band 32 is greater than that in band 31. For this reason, the

negative values of the difference between these two bands indicate the dust and positive values while the values close to zero indicate the temperature of the cloud and other surfaces. The use of the thermal range of electromagnetic waves provides the ability to capture data over-night and also cause climate factors to have the least effect on the recovery of infrared waves (Taghavi et al., 2017). Brightness temperature is a descriptive measure of radiation in terms of the temperature of a hypothetical blackbody emitting an identical amount of radiation at the same wavelength (NASA GES DISC 2017). For a black body, Planck's law gives

$$B_{\lambda}(T) = \frac{2\pi hc^2}{\lambda^5 (\exp(\frac{hc}{\lambda kT}) - 1)} \quad (1)$$

where B_{λ} is the black body's irradiance, T is the temperature of the black body, h : 6.6265×10^{-34} JS is Planck's constant, λ represents the wavelength (μm), C : 2.998×10^8 M/S is the speed of light, and K : $1.3806558 \times 10^{-23}$ J/K is Boltzmann's constant. This equation is used to estimate the brightness temperatures from radiances of the satellite sensors, like MODIS. To calculate the brightness temperature of MODIS bands, the coefficients K_1 and K_2 require that the values of these coefficients be calculated via Equations 2 and 3 (Smith, 2005):

$$K_1 = 2hc^2 \lambda^{-1} \quad (2)$$

$$K_2 = hc / K\lambda \quad (3)$$

For a grey body, the spectral radiance is a portion of the black body radiance, determined by the emissivity ε ; that makes the reciprocal of the brightness temperature:

$$T = \frac{hc}{\lambda_i k \ln(\frac{2hc^2}{L(\lambda_i) \lambda_i^5 \varepsilon})} + 1 \quad (4)$$

where L is radiance of λ_i wavelength.

$$BTD(31 - 32) = BTD31 - BTD32 \quad (5)$$

where BTD31 and BTD32 are brightness temperature differences of MODIS band 31 and band 31, respectively. Furthermore, Brightness temperature of bands 20 and 23 were used to calculate BTD (20-31) and BTD (23-31).

Table 1. An example of coefficients calculation of bands 31 and 32 MODIS (Smith, 2005)

Sensor	Band	Wavelength (μm)	Mean (μm)	$K_1 \times 10^{-7}$	K_1 (Micron)	K_1 (Kelvin)
Example			10	119.10	1191.04	1438.76
MODIS	31	10.78-11.28	11.03	72.96	729.57	1304.40
MODIS	32	11.77-12.27	12.02	47.47	474.71	1197.00

Several BTD indices with different thresholds, including BTD (20-31), BTD (23-31), and BTD (31-32), were used to detect the dust over-night.

Determination of samples and spectral specifications

In this part of the method, we tried to show the mean and standard deviation of BT and BTD for clouds and dust events used in ANN training and validation (Table 2) and the mean and

standard deviation of BT and BTD for clouds and dust events used in ANN training and validation (Table 3).

Table 2. Mean and standard deviation of BT and BTD for clouds and dust events used in ANN training and validation

Events	Statistics	BT32	BT31	BT23	BT20	BTD32-31	BTD23-31	BTD20-31
Cloud	MEAN	256.78	257.49	257.09	255.41	-0.71	-0.40	-2.08
	STD	16.45	16.80	16.26	16.36	0.65	0.91	0.96
Dust	MEAN	290.78	290.56	289.11	287.63	-0.57	-1.45	-2.93
	STD	11.51	11.36	9.59	9.62	1.27	2.26	2.49

Table 3. Mean and standard deviation of surface reflectance in band 1-band 7 for land, vegetation, water used in ANN training, and validation

Events	Statistics	b1	b2	b3	b4	b5	b6	b7
Land	MEAN	0.319	0.243	0.147	0.100	0.444	0.480	0.436
	STD	0.079	0.080	0.036	0.053	0.093	0.107	0.114
Vegetation	MEAN	0.112	0.398	0.058	0.233	0.239	0.202	0.140
	STD	0.040	0.079	0.018	0.029	0.077	0.074	0.064
Water	MEAN	0.024	0.016	0.038	0.046	0.017	0.029	0.025
	STD	0.059	0.065	0.039	0.056	0.070	0.074	0.067

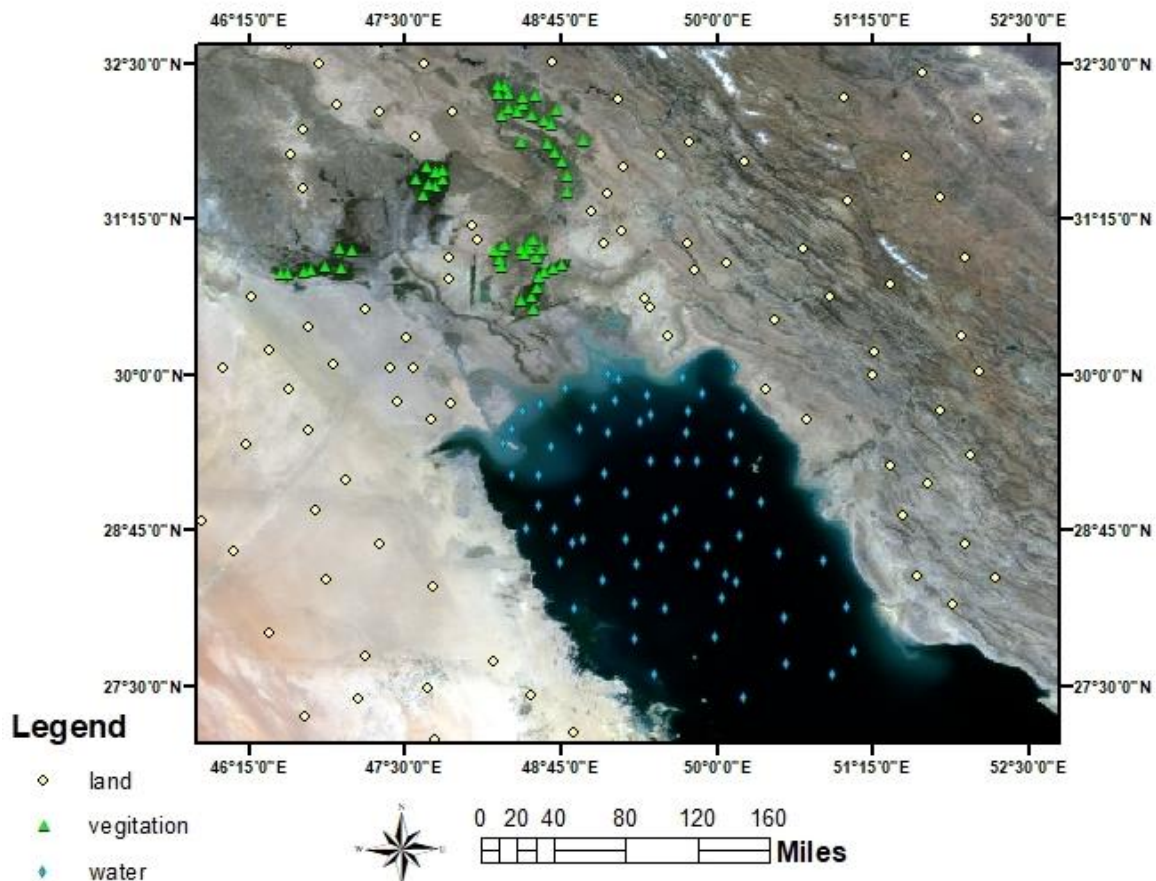


Figure 3. Sampling point

Figure 3 depicts a number of sampling points of water, soil, and vegetation of the study area.

Artificial neural network (ANN)

An ANN system was utilized to classify MODIS images. The parameters used to train ANN were the signals from clouds, dust, soil, and water in different wavelengths. To obtain an optimized ANN architecture in terms of the total number of neurons and hidden layers, a simple ANN architecture was initially considered. Subsequently, the errors of ANN were compared based on the increase in the neurons and hidden layers in order to obtain a more accurate ANN. The main purpose of the training process was to minimize the error between ANN output and input data by adjusting the correlation weights among them. Finally, a network design with three layers, namely (a) four input layers, (b) 10 neuron hidden layers, and (c) two output layers, was employed in this study. It is also worth mentioning that 80%, 10%, and 10% of all the samples were randomly used for training, testing, and validation, respectively. Finally, different indices were used for accuracy assessments.

Validation

To evaluate the results of the accuracy of BTD and ANN approaches, different indices were calculated, including RPT, RPF, TNR, FNR, ACC, PPV, NPV, and FDR. The True Positive Rate (RPT) is a number of dust samples that are properly classified in the dust class; a larger number represents a better prediction. The False Positive Rate (RPF) is a number of non-dust samples that are mistakenly classified in the dust class; a lower number indicates a better performance. The True Negative Rate (TNR) is a number of non-dust samples that are categorized correctly in the non-dust class; a higher number indicates a better performance. The False Negative Rate (FNR) is a number of dust samples that are mistakenly classified in non-dust classes; a lower number indicates a better performance. Achieve High Accuracy index (ACC) indicates a better performance. Positive Predictive Value (PPV) detects the dust, in which a higher number represents a better performance. The Negative Predictive Value (NPV) identifies non-dust as non-dust, in which a higher number represents a better performance. The False Discovery Rate (FDR) detects non-dusting as a non-dust source, in which the lower number indicates a better performance. Here ΣTP and ΣTN are the correct positive and negative integer pixels; ΣFP and ΣFN are false positive and false negative pixels, respectively. All these predictive measures are interconnected and independent of each other (El-Ossta, 2013), the equations are:

$$FN + TP (\Sigma / TP \Sigma = TPR) \quad (6)$$

$$FPR = \Sigma FP / \Sigma (FP + TN) \quad (7)$$

$$TNR = \Sigma TN / \Sigma (TN + FP) \quad (8)$$

$$FNR = \Sigma FN / \Sigma (FN + TP) \quad (9)$$

$$ACC = (\Sigma TP + TN) / \Sigma (TP + FP + TN + FN) \quad (10)$$

$$PPV = \Sigma TP / \Sigma (TP + FP) \quad (11)$$

$$NPV = \Sigma TN / \Sigma (TN + FN) \quad (12)$$

$$FDR = \Sigma FP / \Sigma (TP + FP) \quad (13)$$

$$FPR + TNR = 1 \quad (14)$$

$$TPR + FNR = 1 \quad (15)$$

$$PPV + FDR = 1 \quad (16)$$

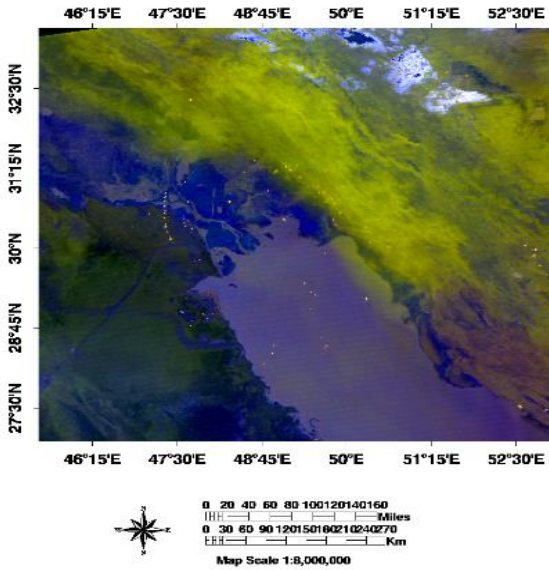
To use the artificial neural network, 80%, 10%, and 10% sample images were utilized for train, test and validation processes, respectively.

Results

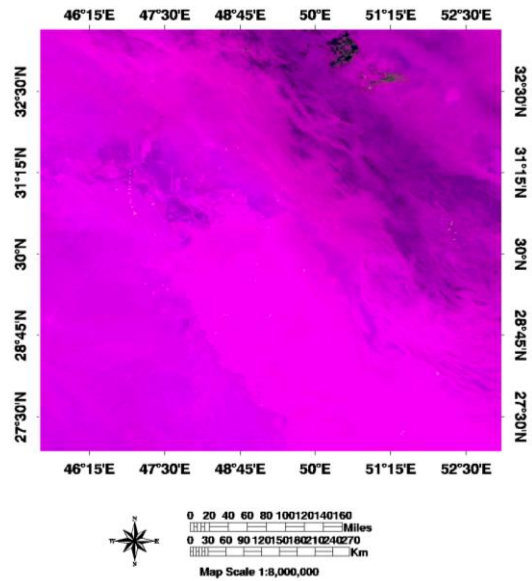
Dust detection in over-night images is possible through calculating the brightness temperature. Dust phenomena can be identified by creating false color combinations of BT (31-20), BT (31-23), and BT (32-31). In order to evaluate the methods, a few over-night images were considered and BT indices and ANN method were utilized to detect dust. Ultimately, the accuracy of the implemented methods was assessed.

Dust storm on July 2, 2008

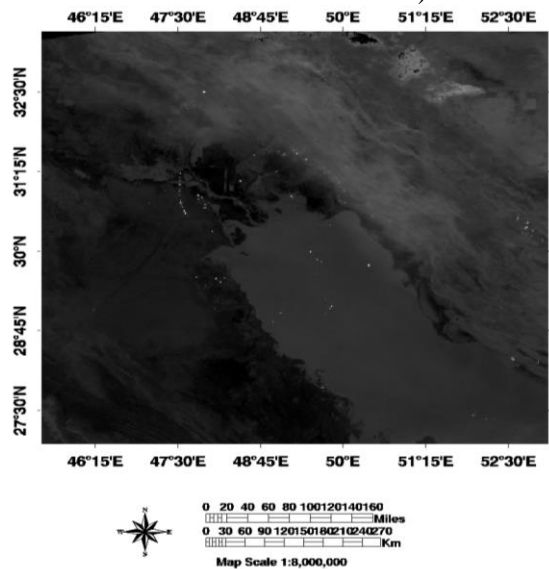
This over-night image was captured on July 2, 2008, which was selected from the Aqua Satellite MODIS Sensor.



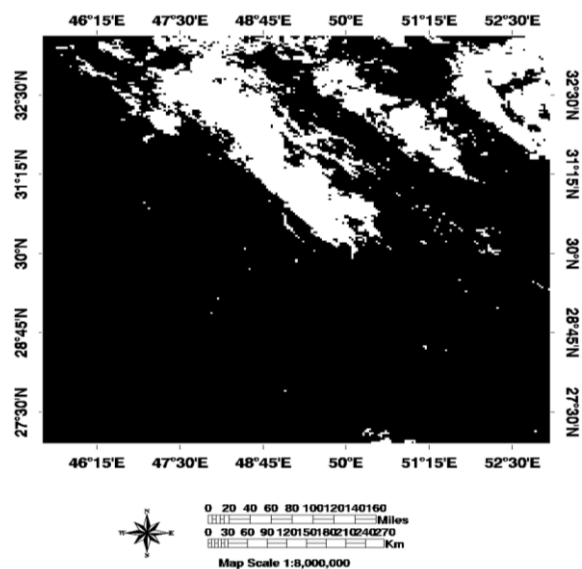
A. False color combination of BT (20-31), BT (23-31), and BT (31-32) (the yellow area indicates a dust storm)



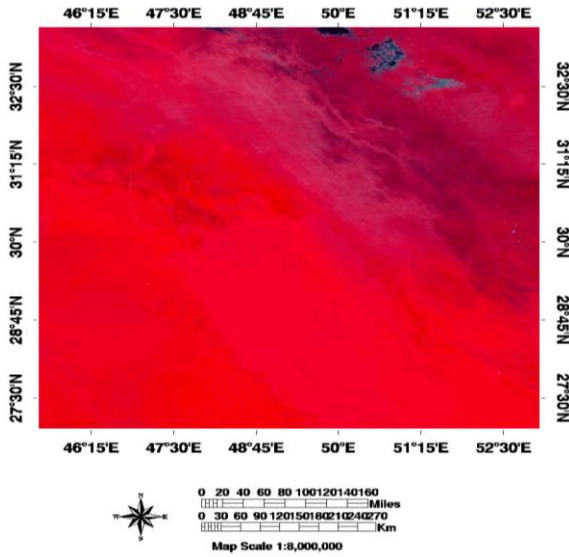
B. False color combination BT (20-31)



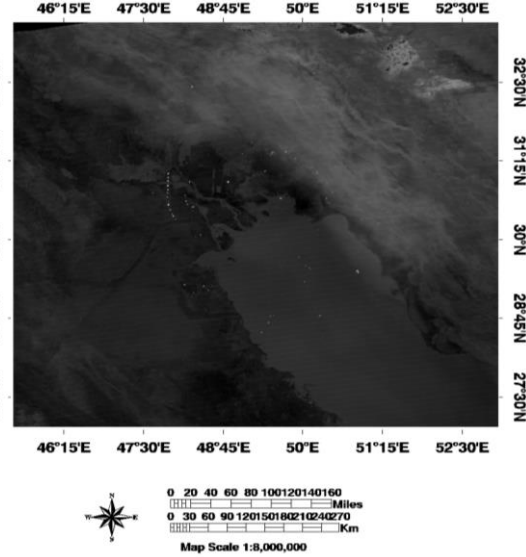
C. The result of BT (20-31)



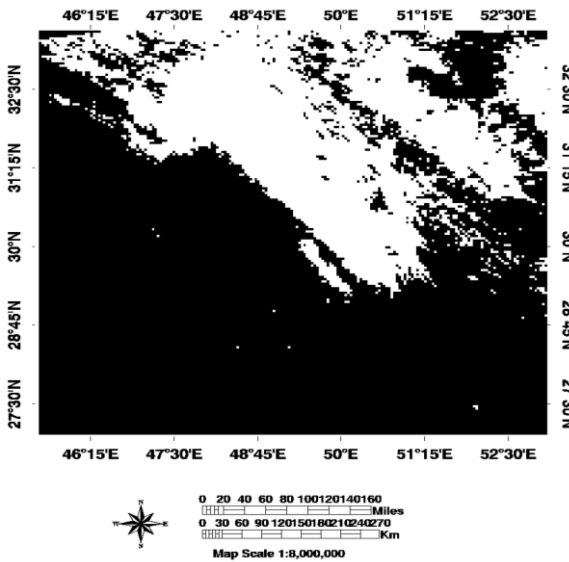
D. Dust mask with threshold $BT(20-31) > 4$



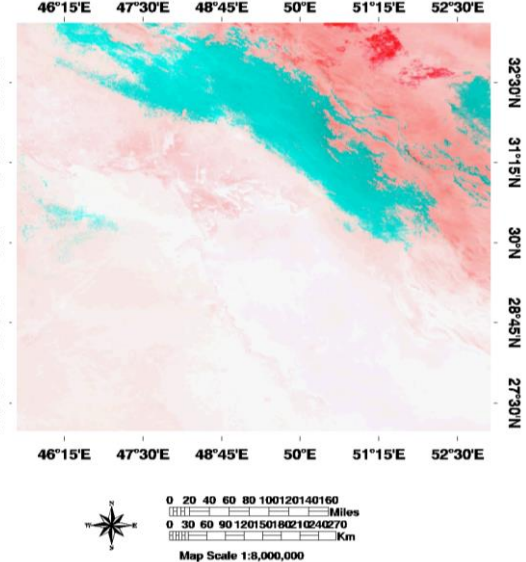
E. False color combination BTM (23-31)



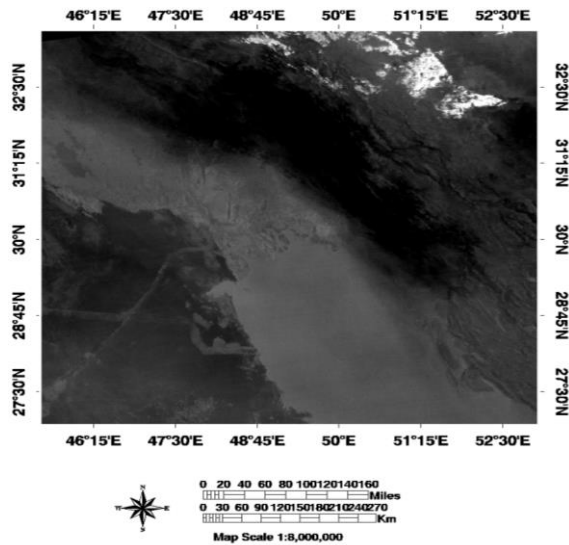
F. The result of BTM (23-31)



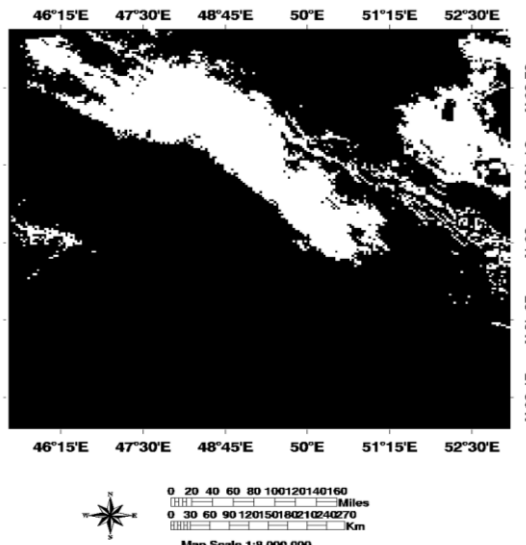
G. Dust mask with threshold $BTM(23-31) > 0$



H. False color combination BTM (31-32)



I. The result of BTM (31-32)



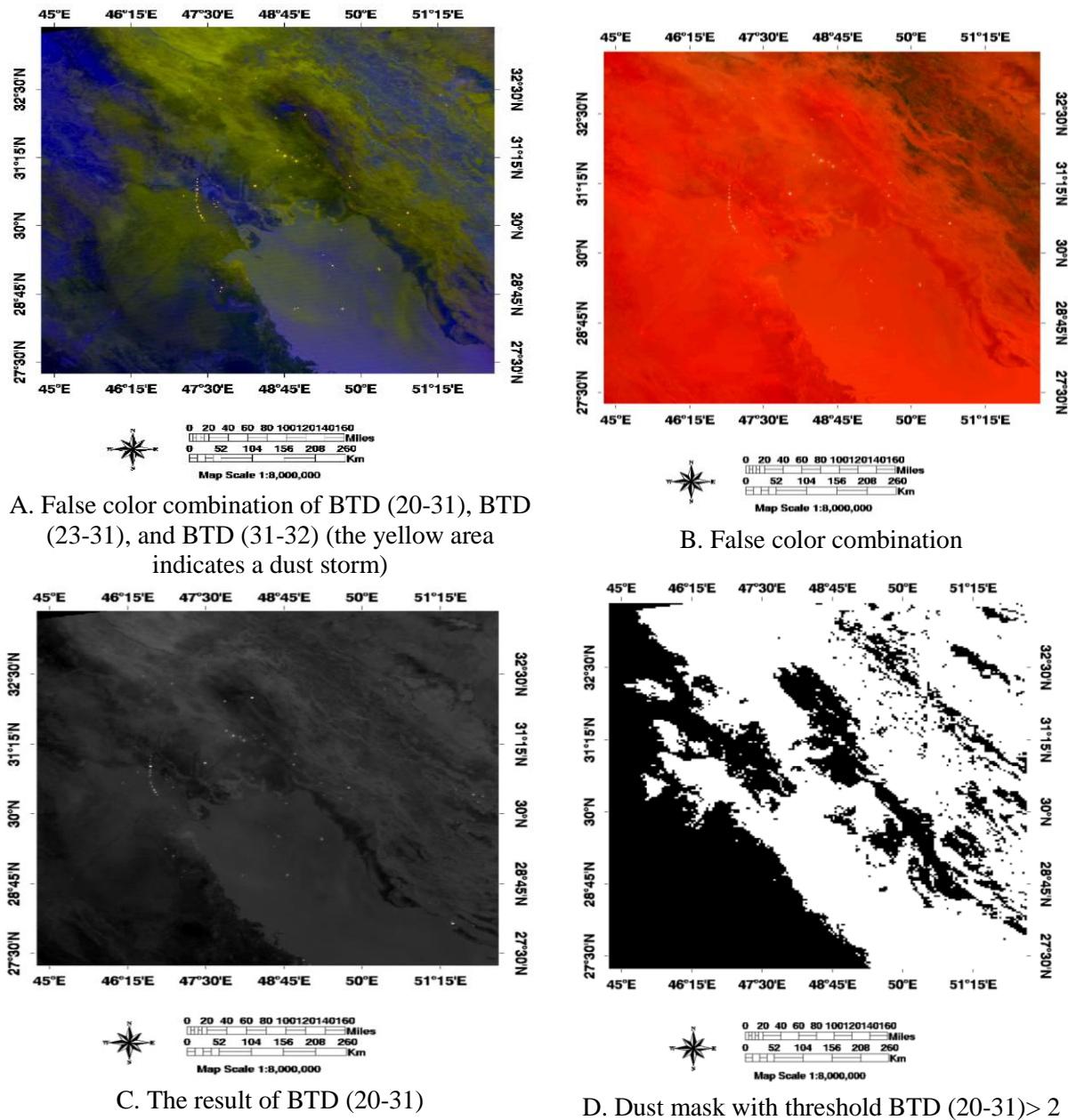
M. Dust mask with threshold $BTM(31-32) < -1$

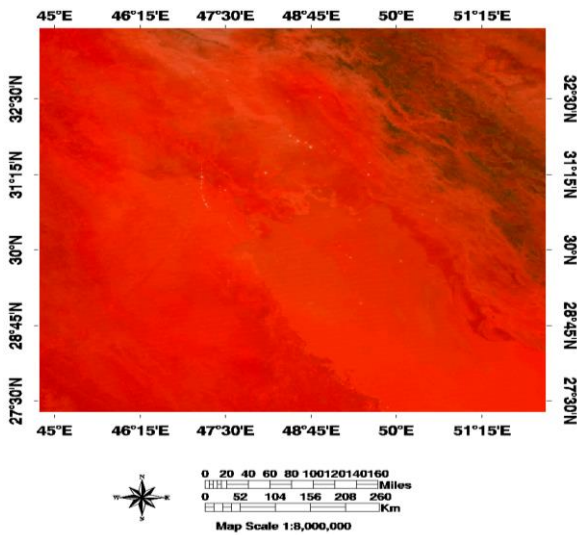
Figure 4. The results of applying BTD (20-31), BTD (23-31), and BTD (31-32) for the dust storm on July 2, 2008

Figure 4 illustrates the results of BTD indices with different thresholds implemented on the over-night MODIS image captured on July 2, 2008. The accuracy of the results obtained from several indices with different thresholds values were in the following order: BTD (20-31) with 91.02% accuracy > the BTD (23-31) with 82.13% accuracy > BTD (31-32) with 65.19% accuracy.

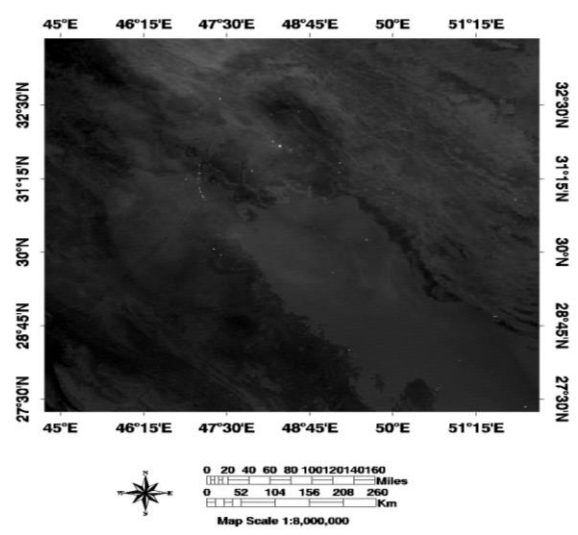
Dust storm on July 5, 2009

This over-night image was captured on July 5, 2009, which was selected from the Terra Satellite MODIS Sensor.

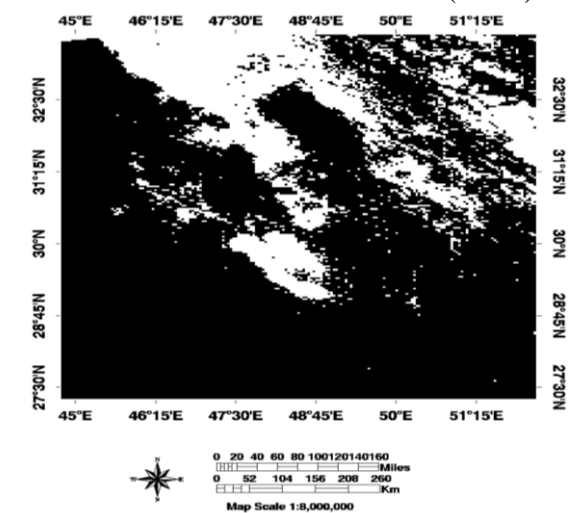




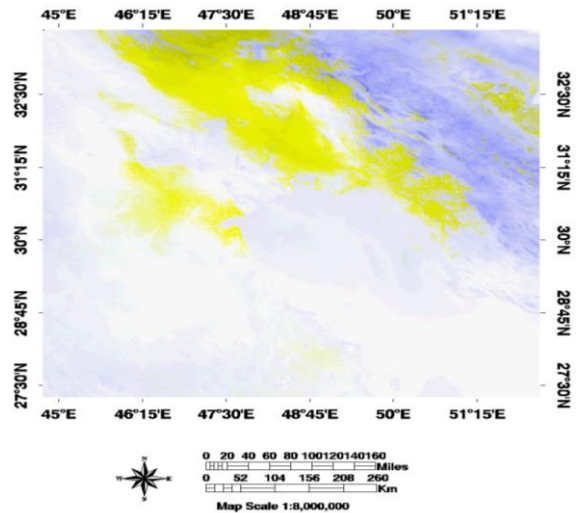
E. False color combination BTD (23-31)



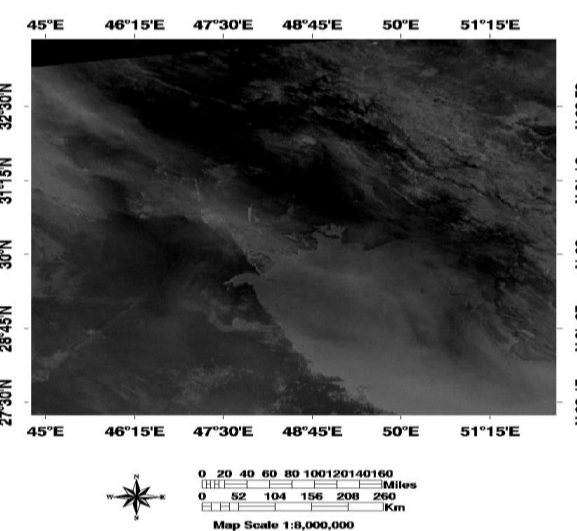
F. The result of BTD (23-31)



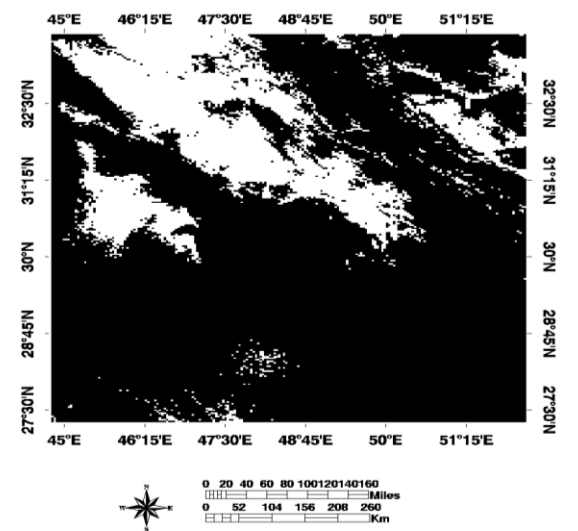
G. Dust mask with threshold $BTD(23-31) > -0.5$



H. False color combination BTD (31-32)



I. The result of BTD (31-32)



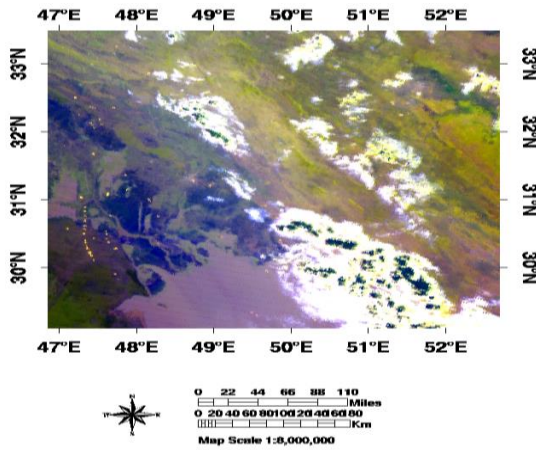
M. Dust mask with threshold $BTD(31-32) < -1$

Figure 5. The results of applying BTD (20-31), BTD (23-31), and BTD (31-32) for the dust storm on July 5, 2009

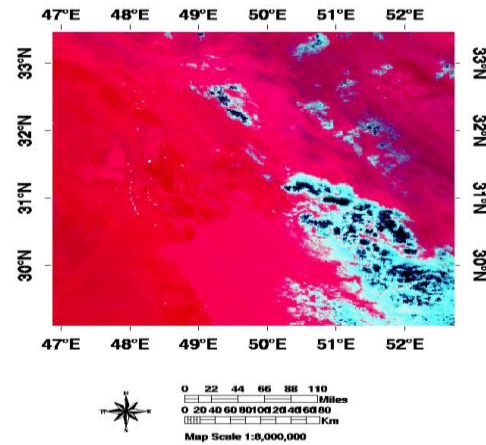
Figure 5 demonstrates the results of BTD indices with different thresholds implemented on the over-night MODIS image captured on July 5, 2009. The accuracy of these results are in the following order: BTD (20-31) with an accuracy of 82.71% > the BTD (23-31) with an accuracy of 83.77% > BTD (31-32) with an accuracy of 60.63%.

Dust storm on July 14, 2014

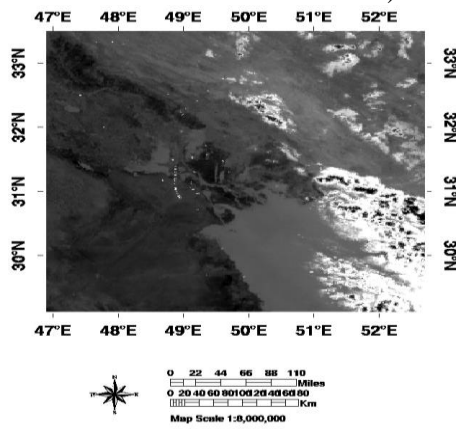
This over-night image captured on July 5, 2009, which was selected from the Aqua Satellite MODIS Sensor. In this image, the concentration and volume of dust is low.



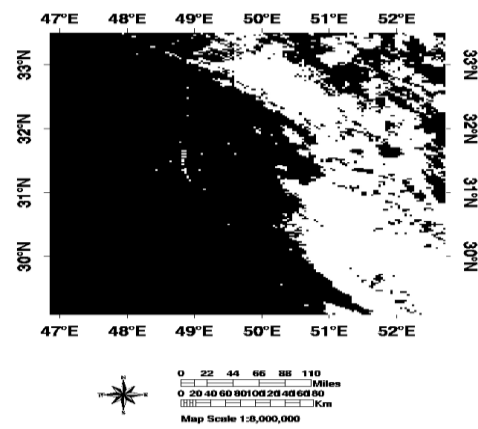
A. False color combination of BTD (20-31), BTD (23-31), and BTD (31-32) (the yellow area indicates a dust storm)



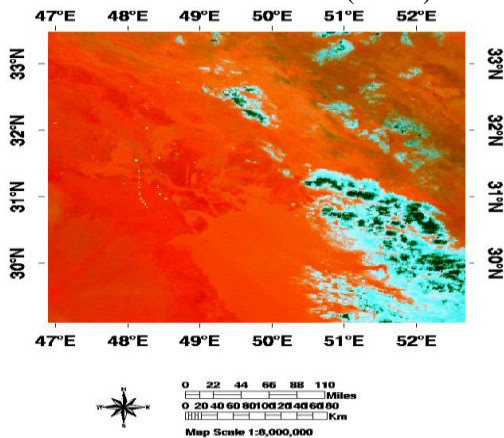
B. False color combination



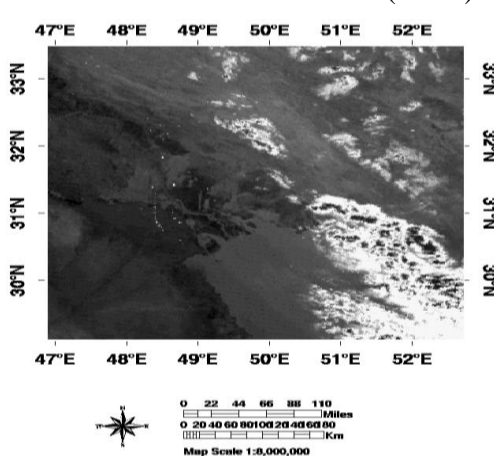
C. The result of BTD (20-31)



D. Dust mask with threshold BTD (20-31) > 2.5



E. False color combination BTD (23-31)



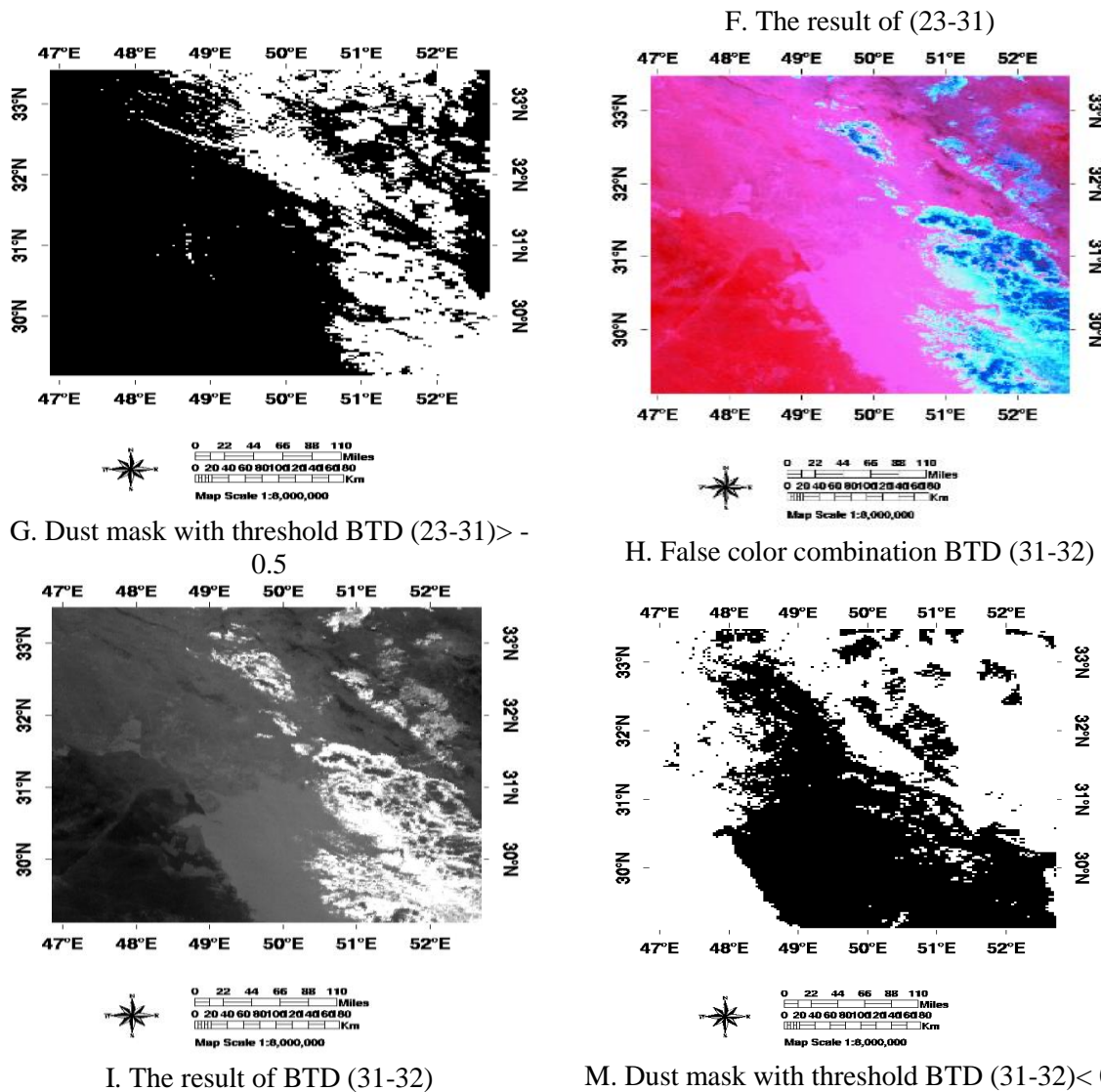


Figure 6. The results of applying BTM (20-31), BTM (23-31), and BTM (31-32) for the dust storm on July 14, 2014

Figure 6 exhibits the results of BTM indices with different thresholds implemented on the over-night MODIS image captured on July 14, 2014. The accuracy is as follows: BTM (20-31) with an accuracy of 90.57% > the BTM (23-31) with an accuracy of 89.06% > BTM (31-32) with an accuracy of 79.06%.

BTM indices evaluation

To evaluate the accuracy of the indices, among the 20 images, different samples of soil, water, cloud, and dust phenomena were selected based on 50 * 50 dimensions. Additionally, the capabilities of BTM indices and ANN to detect dust over-night were assessed by implementing the evaluation indices.

Table 4. BTM indices evaluation

	TPR	FPR	TNR	FNR	ACC	PPV	NPV	FDR
Mean	0.0018	0.2806	0.7194	0.9982	0.4326	0.0043	0.5194	0.9957
STDEV	0	0.0188	0.1880	0	0.0112	0.003	0.0065	0.003

In the Dust Detection Method using the BTD index, determining the threshold corresponded to the area has an important role in representing the dust. The value of the ACC parameter shows that the BTD index had a fairly good accuracy and performance with a value of 43%. Moreover, a rise in the precision of the threshold increases the accuracy. The smaller values of the standard deviation indicate the better performance of the index.

Artificial neural network results

In this study, 192500 datasets, 20 night images, four input layers, 10 neurons in the hidden layer, and two output layers were used to implement the neural network. Figure 7 shows the neural network training, which can be employed to examine the network performance from the plots section. Figure 7 also represents the correlation coefficient graphs. The correlation coefficients of training, evaluation, test, and total data were equal to $R=0.88825$, $R=0.88572$, $R=0.88419$, and $R=0.88726$, respectively, which shows the proper network performance. Different inputs were entered into the network and divided into two classes of dust (0.9) and non-dust (0.1).

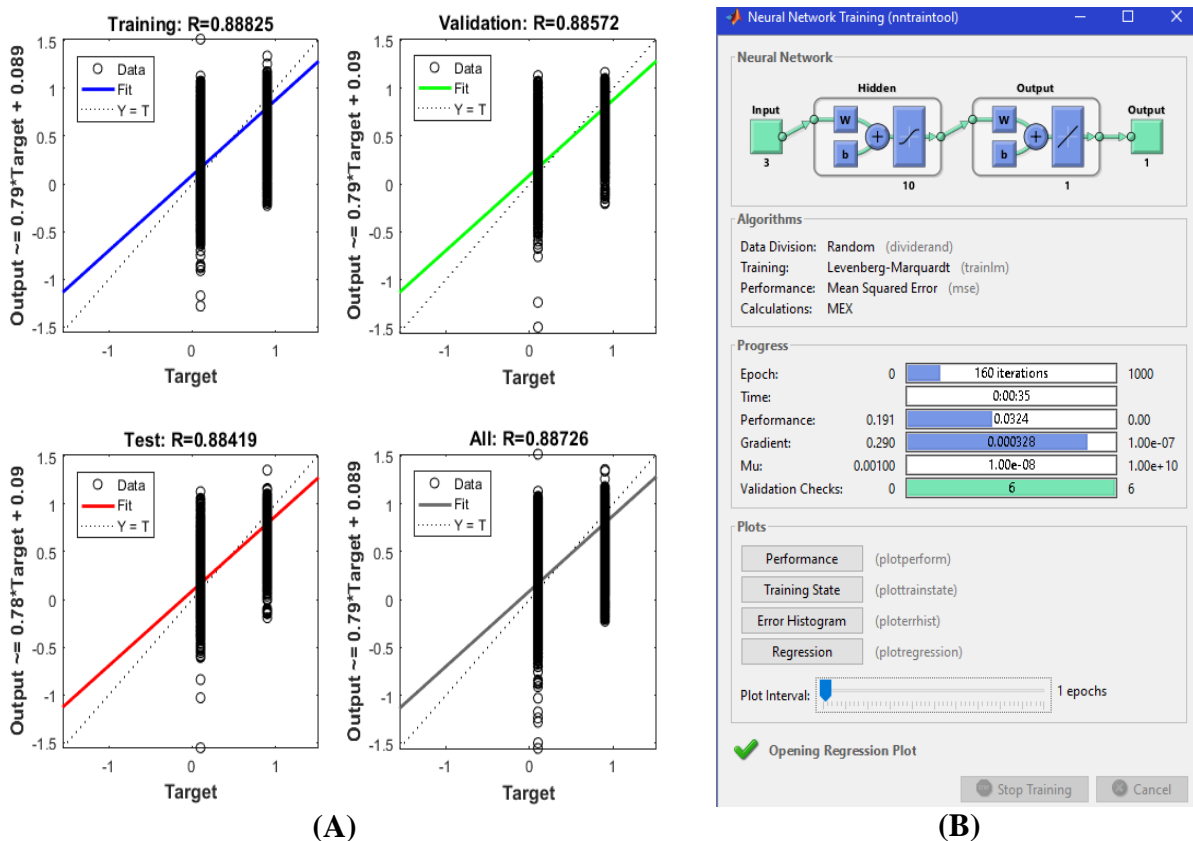


Figure 7. (A) Neural network training of night data; (B) Correlation coefficient (R) for total data, training, evaluation, and night-time test

Figure 8 depicts the accuracy and performance of training, which shows the trend of the mean square error of the network. As explained in the previous section, the error starts from a large value and then gradually decreases, indicating the progress of the network training process. After 154 repeated steps, the network ended in training.

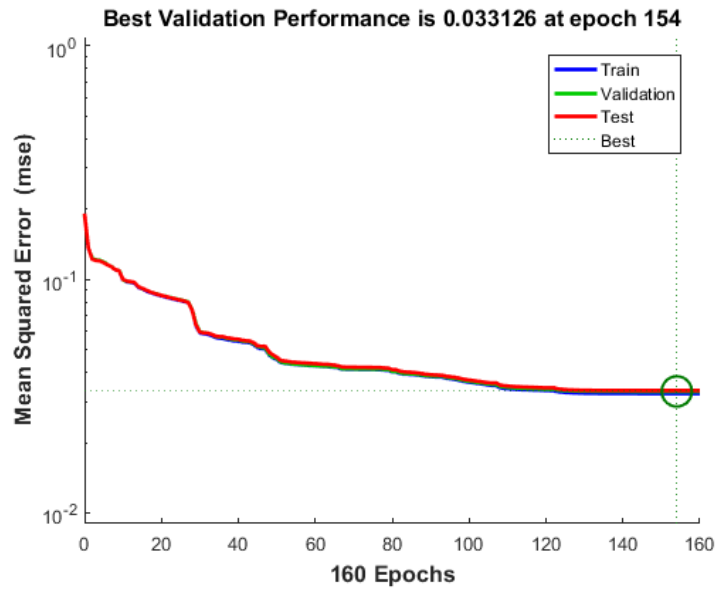
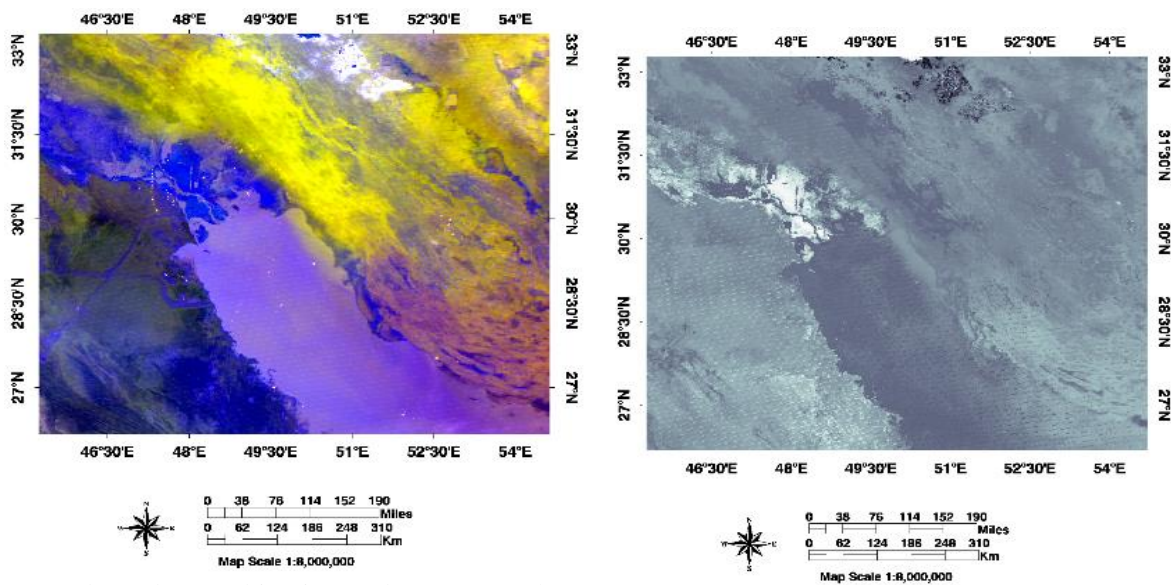


Figure 8. Neural network performance diagram (error) on three sets of training, evaluation, and test data sets

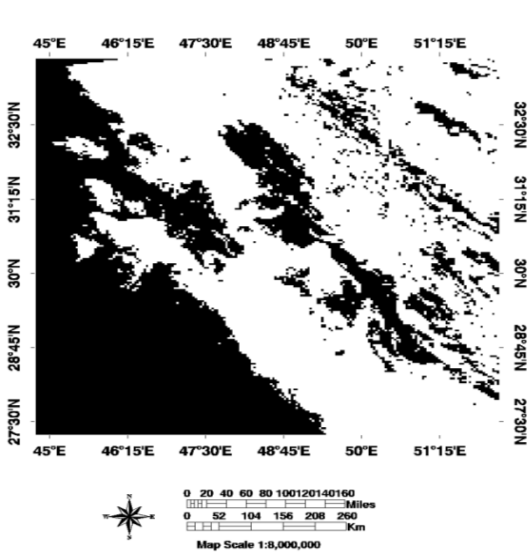
Artificial neural network dust mask

Dust detection over-night is almost troublesome and has more limitations than daily images. Since for over-night assessment, only thermal bands of the MODIS sensor are used, the true color combination cannot be used to better detect phenomena. For this purpose, the output of the neural network was compared with the false color combinations of the images. The results are shown in Figures (9).

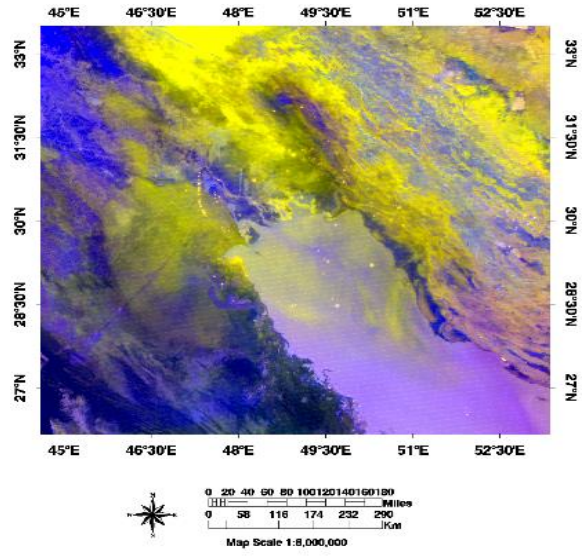


A. False color combination (July 2, 2008) (the yellow area indicates a dust storm)

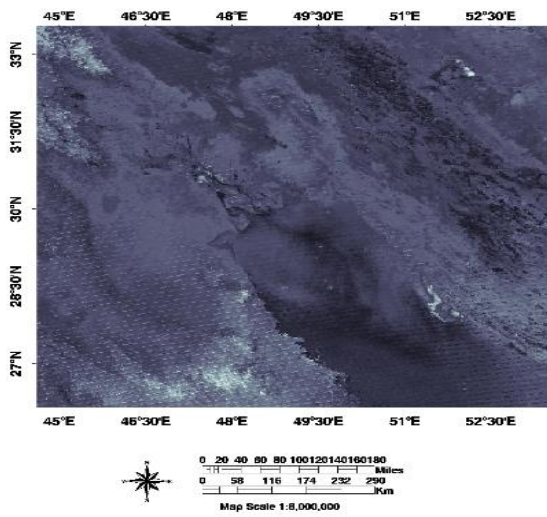
B. Gary scale image (July 2, 2008)



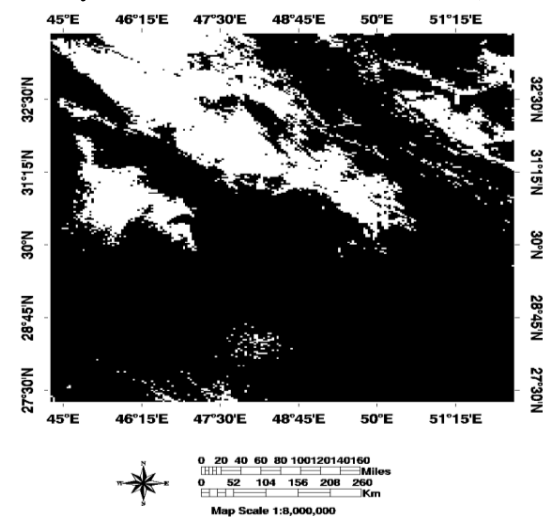
C. ANN dust mask (July 2, 2008)



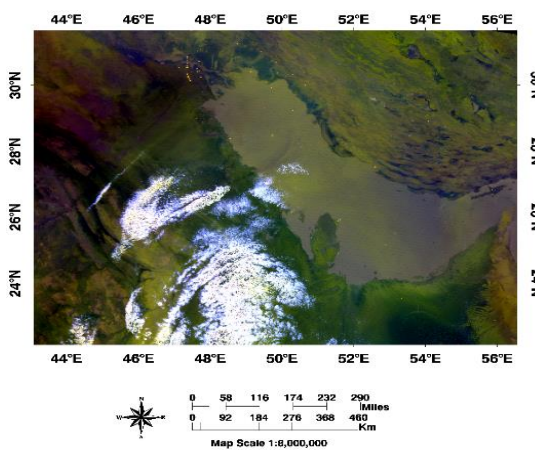
D. False color combination (July 5, 2009) (the yellow area indicates a dust storm)



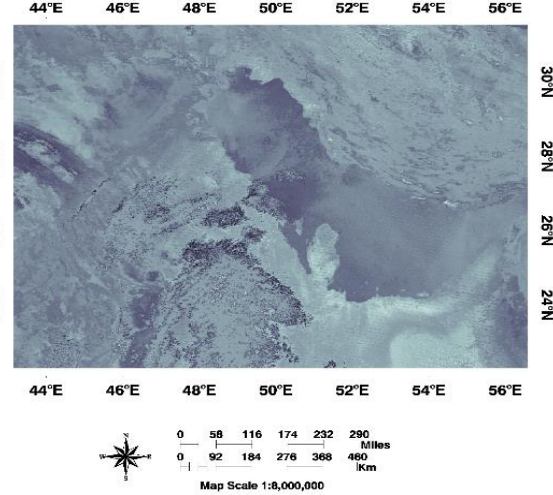
E. Gary scale image (July 5, 2009)



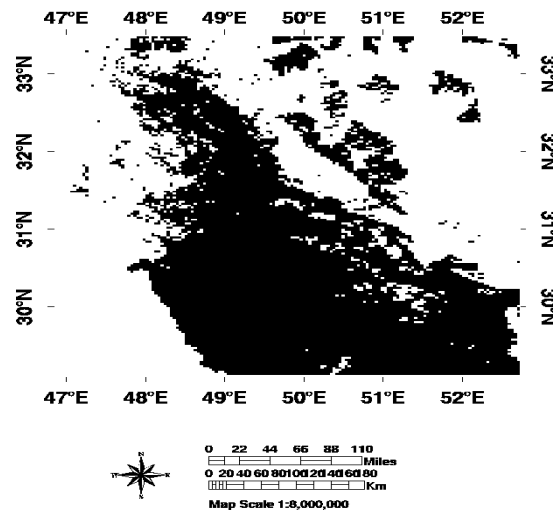
F. ANN dust mask (July 5, 2009)



G. False color combination (July 14, 2014) (the yellow area indicates a dust storm)



H. False color combination (July 14, 2014)



I. ANN dust mask (July 14, 2014)

Figure 9. The results of false color combination, Gray scale image, and ANN dust mask on different dates

Artificial neural network validation

Samples of land, water, cloud, and dust phenomena were selected for training, testing, and validation steps of neural network and different indices were calculated (Table 5).

Table 5. Artificial neural network validation indices

	TPR	FPR	TNR	FNR	ACC	PPV	NPV	FDR
Mean	0.0196	0.0287	0.9733	0.9804	0.5906	0.3776	0.5977	0.6224
STDEV	0.0134	0.0271	0.0254	0.0134	0.0116	0.1030	0.0040	0.1030

Table 3 shows the accuracy results of ANN that implies a fairly good performance for automatic dust detection. Over-night viewing is subject to limitations since the true color combination of the images cannot be utilized to better detect over night dust storm; thus, the samples of the phenomenon should be carefully selected, which highly contributes to the better performance of ANN.

Discussion

Creating a false color combination makes it easier to distinguish between thermal bands for detecting dust in over-night data which cannot be used with natural color images, and also reduce the detection error. It is possible to detect dust well by applying differences between thermal band of BTD (21-31), BTD (23-31), and BTD (31-32) and appropriate thresholds. Proper thresholds have an important role in making BTD indices more accurately. In the present study, in BTD (32-31) of most images, the threshold (-1) could well break the cloud from dust; however, zero threshold mostly detected clouds rather than dust. The visualization was well done in both aquatic and terrestrial ecosystems. The results revealed that the indices with a specified threshold had a fairly good performance of about 43% for the dust detection from other phenomena. Furthermore, the BTD indices results, compared with false color combinations at the night, showed that the BTD index is almost high; meanwhile, from one image to another, this could vary due to the differences in cloud cover conditions, surface reflection, and changes in dust characteristics (altitude and mineral structure particles). In general, the results of this study could not be generalized to the entire region since in each

region; the specific climatic conditions play pivotal roles. Dust enters from different sources; also seems to change this threshold by altering the minerals particales form the dust mass. In addition, surface conditions may alter the value of threshold. As a result, dust detection would be more accurate by increasing the concentration and density of the dust layer, which reduces the amount of cloud, water, and sandy lands in the study area. The results of applying the BTM index herein are consistent with those of other researchers (Bahrami et al., 2020; Shi et al., 2020; Boroughani et al., 2020; Sarikhani et al., 2020; Yang et al., 2017; Cao et al., 2015; Komeilian et al., 2014; Hao and Qu, 2007).

Imagery data, as an input for Artificial neural networks (ANN), has been used for environmental monitoring. ANNs can easily integrate the data collected from different remote sensing sources into an efficient algorithm. Notably, the input data in an ANN algorithm do not need to follow a normal distribution to be transformed into the output layers (Elshorbagy and Parasuraman, 2008; Santi et al., 2016).

An ANN system was trained to detect dust via MODIS data over-night. The parameters employed to train ANN were different samples of soil, water, cloud, and dust phenomena. To obtain an optimized ANN system, a simple ANN architecture was performed and the errors of ANN were compared by increasing the neurons and hidden layers. We carried out the training process to minimize the error between ANN output and input data by adjusting weights among them. An ANN system with three layers, namely (a) three input layers, (b) 10 neuron hidden layers, and (c) two output layers, was implemented in this research. For note, 80%, 10%, and 10% of all the samples were randomly used for training, testing, and validation, respectively. Eventually, after collecting and preparing satellite datasets, as well as training the ANN, the model was evaluated with test datasets to detect dust over-night. The obtained results showed that the accuracy of ANN to detect dust over-night was higher than BTM indices, which is probably attributed to the nonlinear behavior of dust and surface properties. Our results are in line with those reported by Xiao et al. (2015) and El-Ossta (2013).

Conclusion

Over the recent years, dust storms with intense drought have put in anger human health and led to socio-economic adverse effects in arid and semi-arid areas of the world. Dust detection and monitoring is the first essential step for reducing these adverse effects. To detect dust, in situ methods are time-consuming, cost-inefficient, and labor intensive. However, remote sensing are believed to be up-to-date and cost-effective, and have large coverage of vast areas. In this study, the advantages of thermal infrared bands were utilized with performing BTM approaches. Moreover, due to the complex properties of dust event, ANN approach was employed. In comparison with BTM approach, ANN indicated a good capability of detecting dust. This finding could be assigned to the complex properties of dust and the capability of artificial neural network to model nonlinear and complex dust and surface properties.

References

- Bahrami H, Homayouni S, Hosseini RS, ZandKarimi A, Safari A. 2020. Efficient dust detection based on spectral and thermal observations of MODIS imagery. *Journal of Applied Remote Sensing*, 14(3); 034513.
- Boroughani M, Pourhashemi S, Hashemi H, Salehi M, Amirahmadi A, Asadi MAZ, Berndtsson R. 2020. Application of remote sensing techniques and machine learning algorithms in dust source detection and dust source susceptibility mapping. *Ecological Informatics*, 56; 101059.
- Cao H, Amiraslani F, Liu J, Zhou N. 2015. Identification of dust storm source areas in West Asia using multiple environmental datasets. *Science of the Total Environment*, 502; 224-235.

- Chacon-Murguía MI, Quezada-Holguín Y, Rivas-Perea P, Cabrera S. 2011. Dust storm detection using a neural network with uncertainty and ambiguity output analysis. In Mexican Conference on Pattern Recognition, Springer, Berlin, Heidelberg. pp. 305-313.
- El-Ossta EEA. 2013. Automated dust storm detection using satellite images. Development of a computer system for the detection of dust storms from MODIS satellite images and the creation of a new dust storm database. Ph.D. thesis, University of Bradford.
- Elshorbagy A, Parasuraman K. 2008. On the relevance of using artificial neural networks for estimating soil moisture content. *Journal of Hydrology*, 362(1-2), pp.1-18.
<https://doi.org/10.1016/j.jhydrol.2008.08.012>
- Hao X, Qu JJ. 2007. Saharan dust storm detection using moderate resolution imaging spectroradiometer thermal infrared bands. *Journal of Applied Remote Sensing*, 1(1); 013510.
- Hou P, Guo P, Wu P, Wang J, Gangopadhyay A, Zhang Z. 2020. A Deep Learning Model for Detecting Dust in Earth's Atmosphere from Satellite Remote Sensing Data. In 2020 IEEE International Conference on Smart Computing (SMARTCOMP). pp. 196-201.
- Huang J, Ge J, Weng F. 2007. Detection of Asia dust storms using 52 multisensory satellite measurements. *Journal of Remote Sensing of Environment*, 110(2); 186-191.
- Mei DI, Xiushan L, Lin S, Ping WANG. 2008. A dust-storm process dynamic monitoring with multi-temporal MODIS data. *The International Archives of the Photogrammetry, Remote Sensing and Spatial Information Sciences*, 37; 965-970.
- Kamal A, Wu C, Lin Z. 2019. Interannual variations of dust activity in western Iran and their possible mechanisms. *Big Earth Data*, pp.1-16.
- Komeilian H, Ganjidoust H, Khodadadi A. 2014. Parametric analysis for dust plumes modeling using MODIS data over Khuzestan Province, Iran. *Journal of Middle East Applied Science and Technology (JMEAST)*, 20; 704-708.
- Lee J, Shi YR, Cai C, Ciren P, Wang J, Gangopadhyay A, Zhang Z. 2020. Machine Learning Based Algorithms for Global Dust Aerosol Detection from Satellite Images: Inter-Comparisons and Evaluation. UMBC Physics Department.
- Li J, Wong MS, Lee KH, Nichol J, Chan PW. 2020. Review of dust storm detection algorithms for multispectral satellite sensors. *Atmospheric Research*, p.105398.
- Nabavi SO, Haimberger H, Samimi C. 2016. Climatology of dust distribution over West Asia from homogenized remote sensing data. *Journal of Aeolian Research*, 21; 93-107.
- Naimabadi A, Ghadiri A, Idani E, Babaei AA, Alavi N, Shirmardi M, Khodadadi A, Bagherian Marzouni A, Ahmadi Ankali K, Rouhizadeh A, Goudarzi GH. 2016. Chemical composition of PM10 and its in vitro toxicological impacts on lung cells during the Middle Eastern Dust (MED) storms in Ahvaz, Iran. *Journal of Environmental Pollution*, 211; 316-324.
- Park SS, Kim J, Lee J, Lee S, Kim JS, Chang LS, Ou S. 2014. Combined dust detection algorithm by using MODIS infrared channels over East Asia. *Journal of Remote sensing of environment*, 141; 24- 39.
- Sarikhani A, Dehghani M, Karimi-Jashni A, Saadat S. 2020. A New Approach for Dust Storm Detection Using MODIS Data. *Iranian Journal of Science and Technology, Transactions of Civil Engineering*. Pp.1-7.
- Santi E, Paloscia S, Pettinato S, Fontanelli G. 2016. Application of artificial neural networks for the soil moisture retrieval from active and passive microwave spaceborne sensors. *International journal of applied earth observation and geoinformation*, 48, pp.61-73.
- Shi P, Song Q, Patwardhan J, Zhang Z, Wang J. 2020. Mineral dust detection using satellite data. UMBC Physics Department.
- Smith RB. 2005 Computing the Planck Function. Professional Paper, Yale University.
- Taghavi F, Oulad E, Ackerman SA. 2017. Enhancement and identification of dust events in the southwest region of Iran using satellite observations. *Journal of Earth Syst*, 126; 1-28.
- Wu Y, Guo J, Zhang X, Xin T, Zhang J, Wang Y, Duan J, Li X. 2012. Synergy of satellite and ground based observations in estimation of particulate matter in eastern China. *Science of the Total Environment*, 433; 20-30.
- Xiao F, Wong MS, Lee KH, Campbell JR, Shea YK. 2015. Retrieval of dust storm aerosols using an integrated Neural Network model. *Computers & Geosciences*, 85; 104-114.

- Yang Y, Sun L, Zhu Z, Wei J, Su Q, Sun W, Liu F, Shu M. 2017. A simplified Suomi NPP VIIRS dust detection algorithm. *Journal of Atmospheric and Solar-Terrestrial Physics*, 164; 314-323.
- Zhao TXP, Ackerman S, Guo W. 2010. Dust and smoke detection for multi-channel imagers. *Journal of Remote Sensing*, 2(10); 2368-2347.